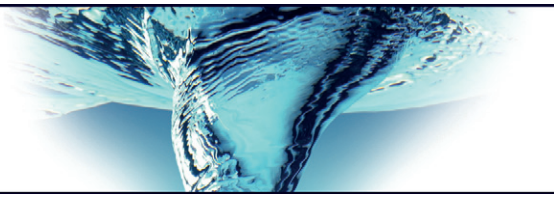
J. Fluid Mech. (2014), *vol.* 744, R1, doi:10.1017/jfm.2014.67

JFM RAPIDS
journals.cambridge.org/rapids



Satellite formation during bubble transition through an interface between immiscible liquids

E. Q. Li[1], S. A. Al-Otaibi[2], I. U. Vakarelski[1] and S. T. Thoroddsen[1,†]

[1]Division of Physical Sciences and Engineering & Clean Combustion Research Center, King Abdullah University of Science and Technology (KAUST), Thuwal, 23955-6900, Saudi Arabia

[2]North Ghawar Producing Department, "Saudi Arabian Oil Company (Saudi Aramco)", Abqaiq, Saudi Arabia

(Received 19 December 2013; revised 18 January 2014; accepted 28 January 2014)

When a bubble rises to an interface between two immiscible liquids, it can pass through the interface, if this is energetically favourable, i.e. the bubble preferring the side of the interface with the lower air–liquid surface tension. Once the intermediate film between the bubble and the interface has drained sufficiently, the bubble makes contact with the interface, forming a triple-line and producing strong capillary waves which travel around the bubble and can pinch off a satellite on the opposite side, akin to the dynamics in the *coalescence cascade*. We identify the critical Ohnesorge numbers where such satellites are produced and characterize their sizes. The total transition time scales with the bubble size and differential surface tension, while the satellite pinch-off time scales with the capillary-inertial time of the pool liquid, which originally surrounds the bubble. We also use high-speed video imaging to study the motion of the neck of the contact. For low viscosity we show that it grows in time with a power-law exponent between 0.44 and 0.50, with a prefactor modified by the net sum of the three interfacial tensions. Increasing the viscosity of the receiving liquid drop drastically slows down the motion of the triple-line, when the Ohnesorge number exceeds $\sim$0.08. This differs qualitatively from the coalescence of two miscible drops of different viscosities, where the lower viscosity sets the coalescence speed. We thereby propose a strong resistance from the triple-line.

Key words: breakup/coalescence, bubble dynamics, capillary flows

1. Introduction

The coalescence of drops or bubbles is the fundamental process occurring during the coarsening of emulsions and foams. However, the coalescence dynamics often produce

† Email address for correspondence: sigurdur.thoroddsen@kaust.edu.sa

© Cambridge University Press 2014

https://doi.org/10.1017/jfm.2014.67 Published online by Cambridge University Press

satellites, when capillary waves focus on the opposite side of the coalescing masses (Charles & Mason 1960). These satellites can have detrimental effects on industrial processes, such as during gas floatation used in oil/water separation.

For low-viscosity liquids these coalescence dynamics allow multiple self-similar steps in the *coalescence cascade*, demonstrated by Thoroddsen & Takehara (2000). Viscosity eventually stops the partial coalescence for the smallest drops, as characterized by Blanchette & Bigioni (2006), Gilet *et al.* (2007) and Blanchette & Bigioni (2009). Partial coalescence has also been observed for a variety of other configurations: e.g. for drops of different sizes by Zhang *et al.* (2009); for regular (Chen *et al.* 2006; Honey & Kavehpour 2006; Blanchette *et al.* 2009; Ray *et al.* 2010) and non-Newtonian emulsions (Yue *et al.* 2006); for two bubbles, first numerically by Ohnishi *et al.* (1999) and then experimentally by Zhang & Thoroddsen (2008). Furthermore, for a droplet deposited onto a hydrophilic surface, the rapid wetting motion of the contact line can generate waves capable of pinching off satellites, as shown by Roux & Cooper-White (2004), Rioboo *et al.* (2006) and Ding *et al.* (2012).

Herein we present an experimental configuration with similar dynamics, which occurs when a bubble contacts the interface between two immiscible liquids. This produces a triple-line, where the two liquids meet on the bubble surface. The unbalanced surface tensions rapidly pull this triple-line outwards generating capillary waves which travel on the free surface of the bubble. Here again, satellites can be produced by the convergence of these waves. This new configuration has the added complication of three independent surface tensions, the roles of which will be investigated.

2. Experimental setup

2.1. *Glass container and micro-capillaries*

The experimental configuration consists of a small bubble rising towards an interface between two immiscible liquids. Figure 1(*a*) shows a schematic of the setup. The continuous phase in the pool is held inside a square-cross-section glass cuvette with inner dimensions of 4×4 cm. The dispersed immiscible phase in the drop is brought in through a nozzle connected to a syringe. To produce small bubbles we use minuscule capillary tubes made of glass. To fabricate tube openings as small as 2 μm we heat and extend the capillary tubes in a glass puller (P-97 Flaming/Brown type from Sutter Instruments), with original glass capillaries from *World Precision Instruments*. The end of the tube is broken off to open up the hollow interior channel. The air is pushed through the tube and forms a spherical bubble which is pinched off and rises up towards the liquid–liquid interface. The very fine glass channel introduces a large pressure drop in the air flow, which is essential to allow repeatable release of a single small bubble. We use a combination of an air compressor and a pressure regulator (AD 3000D, from Iwashita Instruments Pte Ltd) to supply a sequence of small pressure pulses to build up the bubble for release. By varying the pulse-duration (13–50 ms) a range of bubble sizes can be generated, typically from 60 to 500 μm in diameter.

The droplets are imaged using long-distance microscopes with Mitutoyo objectives 5×, 10× and 20×, with the corresponding pixel resolution of 4.7, 2.4 and 1.2 μm. The rapid surface motions during the coalescence require high-speed video at frame rates up to 620 kfps, acquired with a Phantom V1610 CMOS video camera. Most video clips were acquired at 560 kf.p.s. where the pixel area has been reduced to 64×128 px. Backlighting is applied with a 350 W metal–halide lamp (Sumita Optical Glass, Inc.), which is shone onto a diffuser.

https://doi.org/10.1017/jfm.2014.67 Published online by Cambridge University Press

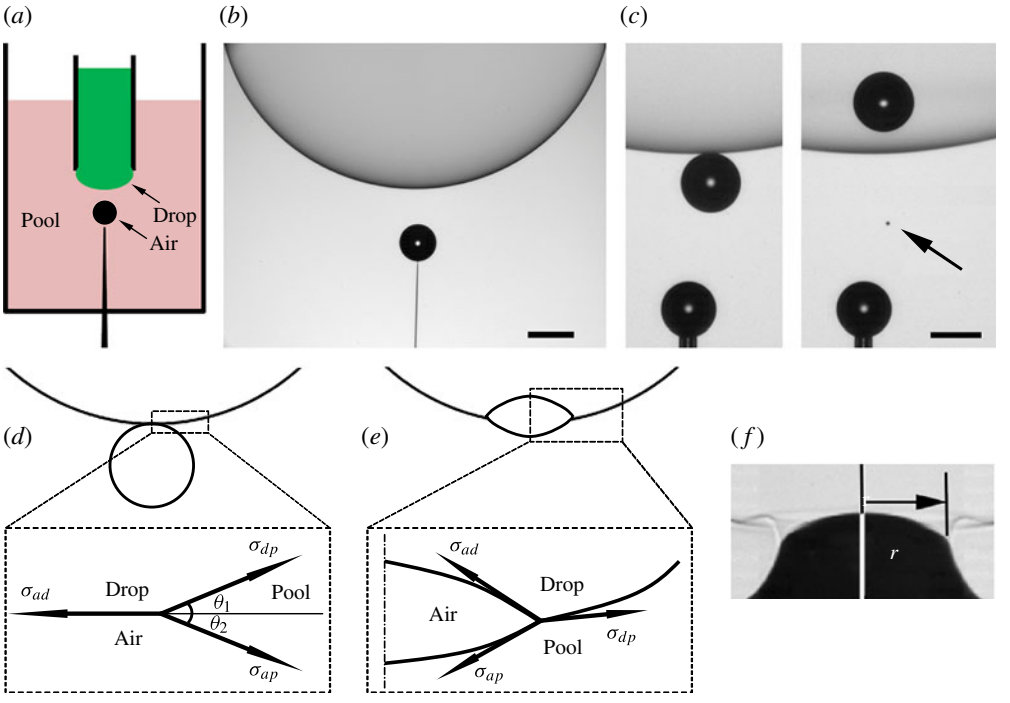


FIGURE 1. (*a*) Sketch of the experimental configuration, showing the capillary micro-tube used to pinch off the air bubble. The continuous phase is here denoted as the *pool* and the dispersed phase is confined at the opening of a syringe denoted as the *drop*. (*b*) Typical setup for salty water and a silicone oil drop, showing the micro-capillary. The scale bar is 500 μm long. (*c*) A bubble passes through the interface leaving a small satellite, marked by the arrow. The time between the frames is 1.5 ms. Scale bar is 200 μm long. (*d*) Definition sketch showing the three interfacial tensions at the triple-line, immediately following first contact and (*e*) at end of the process if the bubble forms a lens. (*f*) Typical close-up video frame used to measure the radius of the minimum contact for a bubble coalescing with the immiscible interface.

2.2. *Liquids*

We limit the current study to bubbles in a low-viscosity pool of water or salt-water solutions. The drop is formed from numerous different immiscible liquids among them a range of silicon oils of various viscosities, perfluorohexane and others, with their properties listed in table 1. Values are only listed for the liquid pairs used in the experiments. Further details for suppliers and chemical codes are given in the online supplementary materials available at http://dx.doi.org/10.1017/jfm.2014.67. The curvature of the drop surface is always much smaller than that of the bubble. The table lists the interfacial tension between the drop liquid and water or salt-water solution. These interfacial tensions are measured using a ring tensiometer (K100 MK2/SF/C, Kruss GmbH, Hamburg).

Some of the immiscible liquid pairs were selected in an attempt to match the refractive index to allow better imaging across the liquid–liquid interface. The work of Smedley & Coles (1990) lists numerous possible matched pairs, but many were excluded due to toxicity or their high viscosity, which dampens the capillary waves and prevents satellite pinch-off.

https://doi.org/10.1017/jfm.2014.67 Published online by Cambridge University Press

Liquid (drop)	Density ρ (g cm^{-3})	Viscosity μ (cP)	IFT σ (dyn cm^{-1})			IFT σ_{net} (dyn cm^{-1})		S
			Air	SS	W	SS (pool)	W (pool)	SS (dyn cm^{-1})
Air (A)	0.0012	0.0186	—	80.0	72.4	—	—	—
Water (W)	0.998	0.981	72.4	—	—	—	—	—
Saturated NaCl Sol. (SS)	1.199	1.98	80.0	—	—	—	—	—
1-Bromopropane (1BR)	1.354	0.542	24.8	31.5	—	86.8	—	23.7
2-Ethylhexyl acetate (2EA)	0.872	1.48	26.6	26.1	—	79.6	—	27.3
Ethyl caprylate (EC)	0.869	1.56	28.1	28.0	—	79.9	—	23.9
Flutec PP1	1.700	1.10	12.4	63.7	55.8	131.2	115.7	3.9
Flutec PP90	1.905	1.67	16.6	62.4	55.6	125.8	111.4	1.0
PDMS 0.65 cSt	0.759	0.493	15.3	47.7	—	112.4	—	17.0
Silicone oil 1.7 cSt	0.866	1.47	17.9	46.5	—	108.7	—	15.6
Silicone oil 2 cSt	0.880	1.76	18.2	46.1	—	107.9	—	15.7
Silicone oil 5 cSt	0.915	4.58	19.3	48.0	—	108.7	—	12.7
Silicone oil 10 cSt	0.935	9.35	19.8	47.0	—	107.2	—	13.2
Silicone oil 30 cSt	0.955	28.6	20.8	47.0	—	106.2	—	12.2
Silicone oil 100 cSt	0.965	96.5	20.9	47.0	—	106.1	—	12.1
Silicone oil 350 cSt	0.970	340	21.1	47.0	—	105.9	—	11.9
Silicone oil 1000 cSt	0.970	970	21.2	47.0	—	105.8	—	11.8

TABLE 1. Properties and interfacial tensions (IFT) of the different liquids used in the experiments. $\Delta\sigma$ is the net sum of the three interfacial tensions, as defined in (3.2). S is the spreading parameter, as defined in (2.2). All interfacial tensions were measured at room temperature 21°C. The chemical suppliers are listed in the online supplementary material available at http://dx.doi.org/10.1017/jfm.2014.67.

In this study we always keep the pool liquid at low viscosity, using either pure water through Milli-Q (internal specific resistance of no less than 18.5 MΩ cm^{-1}) or water/salt solution. We dissolved sodium-chloride (NaCl) salt into the water to try to match the refractive index, to aid the imaging of the liquid–liquid interface.

2.3. *Parameters and surface tension balances*

The bubble sizes used herein are always much smaller than the capillary length $a = \sqrt{\sigma/(\Delta\rho\, g)} \sim 1$ mm. The effects of gravity g on the coalescence dynamics are therefore insignificant, with buoyancy only serving to raise the bubble to the interface, and the initial bubble shape is spherical. Here we use the fluid combination giving the smallest capillary length, i.e. the one with the largest density difference $\Delta\rho$ and smallest surface tension σ. The nozzle holding the drop is small enough that the configuration is stable, even if the drop liquid is heavier than the pool liquid.

The configuration lacks an external velocity scale and the Ohnesorge number becomes the primary non-dimensional number describing the dynamics

$$Oh = \frac{\mu}{\sqrt{\rho\sigma R_b}} \tag{2.1}$$

where R_b is the bubble radius; ρ, μ and σ are the density, dynamic viscosity and surface tension, respectively. However, whether to use the liquid properties ρ and μ of the pool or of the drop, must be determined. Furthermore, in what follows we will study which of the three intrinsic surface tensions is the most relevant.

For the bubble to pass fully through the pool–drop interface, there must be a net release of surface energy, which is required to drive the motions during the transit

https://doi.org/10.1017/jfm.2014.67 Published online by Cambridge University Press

(we show below that buoyancy is insignificant during the rapid motions). Therefore, the surface tension between the air and pool must be higher than between the air and drop, i.e. $\sigma_{ap} > \sigma_{ad}$. However, this is a necessary but not sufficient condition, as the bubble could get trapped at the interface through the interplay with the drop–pool interfacial energy.

It is instructive to first look at the static Newmann conditions at the triple-line, see e.g. de Gennes, Brochard-Wyart & Quéré (2004) or Neeson *et al.* (2012). Here one distinguishes two basic conditions: (i) if $\sigma_{dp} > \sigma_{ap} + \sigma_{ad}$ the bubble could be pulled into a thin air film at the interface. In practice this is quite unlikely, as the surface tension between the liquids and air is usually larger than between the two liquids. (ii) On the other hand, if $\sigma_{dp} < \sigma_{ap} + \sigma_{ad}$ the bubble will remain compact, either as a lens at the interface, or fully within one or other of the liquids. The conditions determining whether the bubble is pulled fully through the interface, or is trapped as a lens, are the following. If $\sigma_{ap} > \sigma_{ad} + \sigma_{dp}$ the triple-line is pulled down along the bubble and cannot find a static equilibrium, even at the bottom apex. The bubble therefore enters the drop (see figure 2). Whereas for $\sigma_{ad} > \sigma_{ap} + \sigma_{dp}$ any triple-line would be pulled up along the bubble, leaving it inside the pool. Table 1 shows that the first of these conditions within (ii) is always satisfied in the liquid combinations tested here. We show this by listing the *spreading parameter* (de Gennes, Brochard-Wyart & Quéré 2004) here defined as

$$S = \sigma_{ap} - \sigma_{ad} - \sigma_{dp} > 0. \tag{2.2}$$

Keep in mind that $S = 0$ is the limiting critical value when the angles at the triple-line are all co-linear and in practice the bubble can still be fully wetted by the drop liquid for S values approaching zero, see figure 1(*e*). For other conditions the bubble would not pass through the interface and no rapid dynamics or satellites, of interest here, were formed.

The above description is based on the static conditions, whereas the inertia and viscous hydrodynamics will determine the dynamical evolution of the instantaneous angles around the triple-line. This is conceptually demonstrated by the pinch-off of the satellite itself, which gives a local minimum in the surface energy, consisting of two spherical air volumes. The dynamics of the coalescence are also constrained by the initial geometry of the interfaces as sketched in figure 1(*d*). At the start of the contact σ_{ap} and σ_{dp} act in the same direction opposing σ_{ad}, with the angles θ_1 and θ_2 approaching 0, while at a later stage the direction of σ_{ap} could change, as is sketched in figure 1(*e*). Figure 1(*e*) shows an image of the dynamic triple-line showing quite different angles from those suggested by the geometry. This is studied further in § 3.2. The speed of the coalescence motions will be affected by the resistance provided by the added mass, which will be a function of time. Viscosity will also slow these motions, as shown in § 3.6.

3. Results

3.1. *Overall transit of the bubble through the interface*

Figure 2 shows the overall deformation following the first contact of the bubble and the drop. The neck grows rapidly producing a capillary wave which travels down the sides of the bubble, far ahead of the apparent triple-line (arrow in 5th panel). When this wave converges at the opposite apex it pinches off a satellite. The triple-line is also driven all around the remaining bubble along with large deformations of the free surface. In this case the bubble passes entirely through the interface in less than 2 ms.

https://doi.org/10.1017/jfm.2014.67 Published online by Cambridge University Press

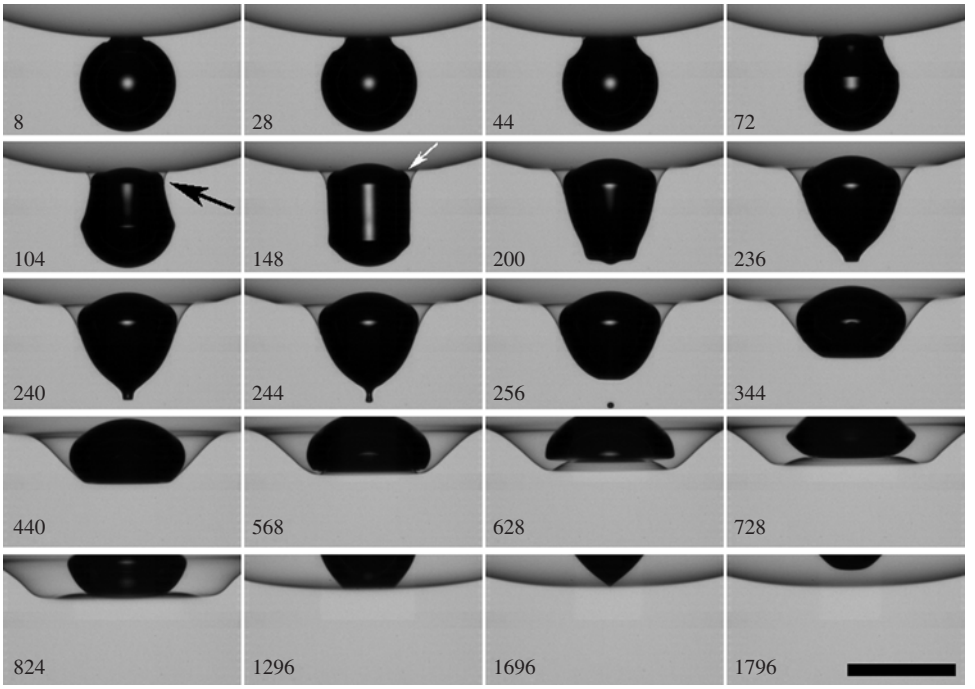


FIGURE 2. Typical sequence of the interface shapes when the bubble touches the interface and pinches off a satellite, while transitioning from salt-water into a 2 cSt silicone oil drop. Times are in μs after first contact. Frames from a video clip taken at 250 kf.p.s.. The initial bubble diameter is 446 μm. The white arrow points to a horizontal dark line, which is due to the index of refraction difference between the two liquids and the axisymmetry of the interface. The scale bar is 500 μm.

Figure 3(*a*) shows the convergence of the triple-line when it has passed around the entire bubble. The shape of this final release of the bubble from the interface depends on the relative properties of the two liquids. In the second-to-last panel in figure 2 the bubble is conical, while the liquid–liquid interface is flat when $\sigma_{dp} = 46$ dyn cm^{-1}, whereas in figure 3(*a–c*) the pool–drop interface is pulled up into a cusp. In figure 3(*a*) the bottom of the air–pool interface is pulled down to form a nipple before it detaches. The threads pulled out of the pool liquid can pinch off a small satellite inside the drop (figure 3*b*). The satellite in figure 3(*b*) is 12 μm in diameter. These threads are only pulled out of the pool if the liquid–liquid interfacial tension σ_{dp} is low compared to the air–drop interfacial tension σ_{ad}, i.e. $\sigma_{dp} \sim 27$ dyn cm^{-1} in figure 3(*b*) and 12.6 dyn cm^{-1} in figure 3(*c*), whereas $\sigma_{ad} \sim 28$ dyn cm^{-1}. This is from a local balance of surface tensions and is observed irrespective of the bubble size in our experiments. For $\sigma_{dp} > 31$ dyn cm^{-1} no threads are pulled out. The bubble transit has thereby entrained a small amount of the pool liquid into the drop and left a small bubble satellite behind inside the pool.

Simple dimensional analysis can give an estimate of the overall time it takes the bubble to transit through the interface. By assuming this process is only dependent on the bubble size R_b, the surface energy released $E_s = (\sigma_{ap} - \sigma_{ad})\, 4\pi R_b^2$ and the added mass of a translating sphere $M = 0.5^2(\rho_d + \rho_p)\, R_b^3\, 4\pi/3$, one can construct a time scale

https://doi.org/10.1017/jfm.2014.67 Published online by Cambridge University Press

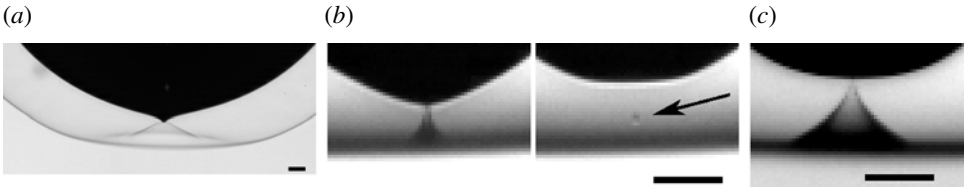


FIGURE 3. Close-up of the tail-end of the pool being pulled into a cusp, for (*a*) a 1,5-pentanediol drop inside a 1-bromooctane pool ($\sigma_{ad} = 43.3$ dyn cm^{-1}, $\sigma_{dp} = 7.0$ dyn cm^{-1}). (*b*) Cusp and thread pinch-off for a 2-ethylhexyl acetate drop in a salt-water solution pool. (*c*) Cusp in a 2-heptanone drop in a salt-water solution pool ($\sigma_{ad} = 24.9$ dyn cm^{-1}, $\sigma_{dp} = 12.6$ dyn cm^{-1}). The scale bars are 100 μm.

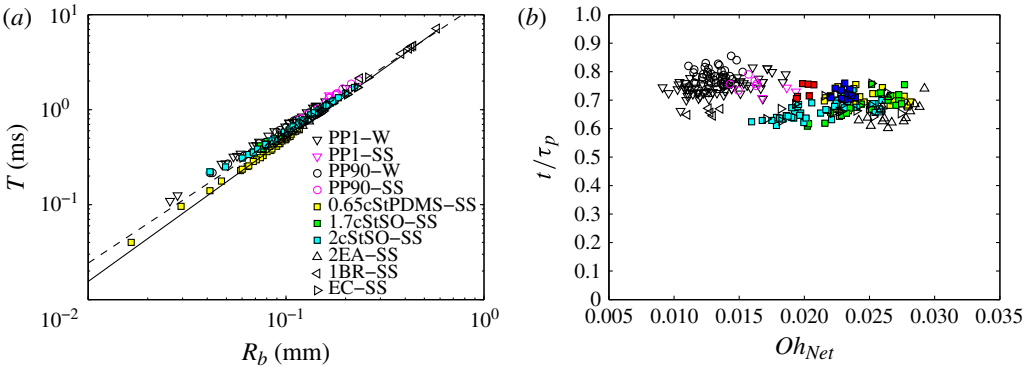


FIGURE 4. The time scales of the coalescence, for low-viscosity drop and pool liquids ($\mu \leqslant 2$ cSt). (*a*) Overall time it takes the bubble to pass through the interface, measured from first contact to the pinch-off of the tail, as in figure 3(*b*). The broken line is a best-fit line of slope 1.38 and the solid line is of slope 1.5. The symbol labels represent the drop–pool liquid combinations, with abbreviations listed in table 1. (*b*) Normalized satellite pinch-off time measured from first contact of the bubble with the interface, until the pinch-off of the satellite bubble, which occurs between panels 10 and 11 in figure 2, versus *Oh* based on the net interfacial tension. Same symbols as in (*a*).

$$T_\sigma = \sqrt{\frac{4MR_b^2}{E_s}} = \sqrt{\frac{R_b^3(\rho_d + \rho_p)}{3\,(\sigma_{ap} - \sigma_{ad})}} \sim 0.5 \text{ ms}, \tag{3.1}$$

which is of the same order as the 1.7 ms in figure 2. Figure 4(*a*) shows a measure of this time, from the first contact to the release of the last cusp (second to last panel in figure 2), for a range of bubble sizes and liquid properties. The best fit to the data gives $T \sim R_b^{1.38}$ which is a somewhat smaller exponent than the value of 1.5 from (3.1). For all of the low-viscosity data we get the following relationship: $T = 2.6\,T_\sigma^{0.92}$.

We note that buoyancy plays only a minor dynamical role as the transition time is too short. Even though buoyancy will accelerate a bubble from rest at twice that due to gravity, the translated distance during time interval T is at most for an inviscid liquid, $dz = 0.5(2g)T^2$, which in figure 2 is only about 5 % of the bubble diameter D_b. The corresponding values of the Bond number $Bo = \rho_p g R_b^2/\sigma$ are small, in the range $\sim 10^{-4}$–10^{-2}, showing the dominant role of surface tension.

https://doi.org/10.1017/jfm.2014.67 Published online by Cambridge University Press

The overall Reynolds number of the bubble transition can be formed by the measured transit time T and a characteristic velocity D_b/T, suggesting a Reynolds number $Re = D_b^2/(\nu_p T) \sim 40$–$140$ (figure 4*a*), which is only weakly dependent on the bubble size, as $T \sim D_b^{3/2}$, thereby giving $Re \sim D_b^{1/2}$.

3.2. *Pinch-off time*

Figure 4(*b*) shows the normalized pinch-off times for all of the liquid combinations which produce satellites. This time interval is measured from the first contact of the bubble with the interface, until the satellite pinches off (Thoroddsen & Takehara 2000). The time is normalized by the capillary inertial time scale based only on the pool properties, i.e. the liquid surrounding the bubble when it makes contact,

$$\tau_p = \sqrt{\frac{\rho_p R_b^3}{\sigma_{ap}}}$$

where R_b is the bubble radius. The data for each liquid pair include different size air bubbles and no apparent trend is observed, when plotted against $Oh_{Net} = \mu/\sqrt{\rho_p R_b(\Delta\sigma/2)}$, the Ohnesorge number based on the net interfacial tension (see figure 1*d*)

$$\Delta\sigma = \sigma_{ap} + \sigma_{dp} - \sigma_{ad}. \tag{3.2}$$

We have used half of $\Delta\sigma$ in the definition of Oh_{Net} to recover earlier definitions for coalescence of two bubbles, where $\sigma_{ap} = \sigma_{dp}$ and $\sigma_{ad} = 0$. The average normalized time for each liquid pair all fall within $t/\tau_p = 0.70 \pm 0.1$. Similar times were observed during the coalescence of two bubbles in Zhang & Thoroddsen (2008), where an average value of 0.68 was recorded, but with a wider spread, attributed to the relative velocity of the two bubbles. In the present experiments the bubbles are much smaller and are always stationary at onset of coalescence.

The relative constancy of the pinch-off time for many different drop liquid properties shows clearly that this time is determined by the wave speed along the bubble–pool interface. However, the drop properties will affect the amplitude of the capillary waves, which influences the satellite size and determines whether a satellite is pinched off or not, i.e. the values of the critical Ohnesorge number Oh, as is shown in the next subsection.

3.3. *Satellite size and critical Ohnesorge number*

Figure 5 shows the satellite size D_s as a fraction of the original bubble size D_b. This is plotted versus the traditional Ohnesorge number defined using the liquid properties of the water pool and σ_{ap} in (2.1). The overall transition from satellite to no pinch-off is more gradual than the sharp jump observed by Zhang & Thoroddsen (2008) during the coalescence of two bubbles. Here the very smallest satellites observed are only $\sim 1.5\,\%$ of the original bubble size. The largest satellites observed in our range of Oh are $12\,\%$ for the lowest values of Oh. This value is similar to those observed for bubble–bubble coalescence. The small size ratio D_s/D_b prevents cascading of bubble coalescences, as Oh increases rapidly during each coalescence stage. However, starting with a very large bubble makes the Bond number $Bo = \rho g R_b^2/\sigma$ so large that it is greatly deformed by gravity.

The data show a large spread in the critical value of Oh from 0.013 to 0.024. For two similar-sized bubbles the corresponding critical value is much smaller at 0.0065

https://doi.org/10.1017/jfm.2014.67 Published online by Cambridge University Press

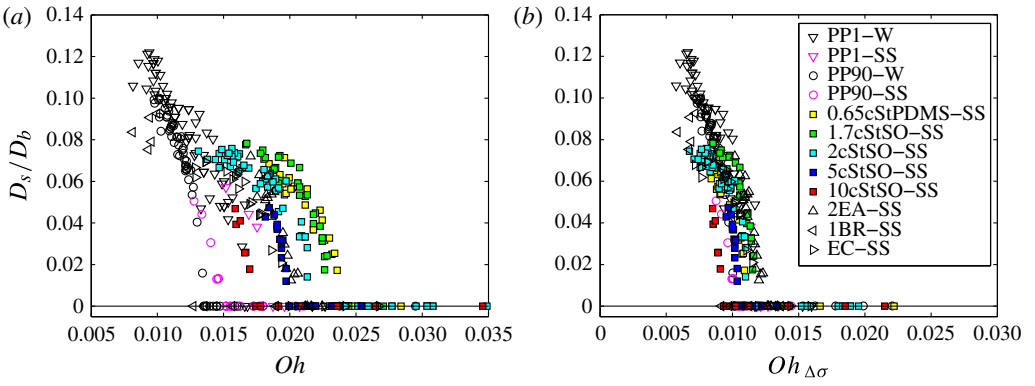


FIGURE 5. The ratio of satellite to original bubble diameters as a function of Ohnesorge numbers. (*a*) Satellite size as a function of Ohnesorge number based on the pool properties. (*b*) Collapse of the data in (*a*) based on the modified $Oh_{\Delta\sigma}$ using the net surface tension at the triple-line and the relative density of the drop.

(Zhang & Thoroddsen 2008). However, in our configuration the dynamics do not only depend on the pool properties, as the drop liquid also plays a role in the production of the capillary waves, during the early stage. We account for this by using the net surface tension $\Delta\sigma$ (3.2). We also modify the *Oh*-definition to include the density ratio of the two liquids:

$$Oh_{\Delta\sigma} = \frac{\mu}{\sqrt{\rho_p R_b\,(\Delta\sigma/2)}}\,\frac{\rho_d}{(\rho_d+\rho_p)}. \tag{3.3}$$

This is an attempt to account for the observation that a denser drop liquid appears to reduce the wave amplitudes and make pinch-off more difficult; figure 5(*a*) shows much smaller critical *Oh* for the heaviest drop liquids (perfluorohexane, i.e. Flutec PP1), than the lightest (0.65 cSt silicone oil). Figure 5(*b*) shows that the data collapse much better using (3.3). The critical value of $Oh_{\Delta\sigma}$ is now in the range from 0.009 to 0.012, with the lowest value due to the most viscous drop.

3.4. *Neck radius versus time*

A separate set of high-speed video sequences was collected at 520 kf.p.s. to track the growth of the neck radius versus time. This extreme frame rate reduced the pixel resolution to 64×128 px, but allowed us to track details of the early neck motions. We first look at the motions for the lowest viscosity liquids. Figure 2 shows that the outwards coalescence motion in the neck is mostly over in 150 μs. Figure 6(*a*) shows the neck growth for three different drop liquids of widely different densities, while keeping the same salt-water solution in the pool. All three show identical behaviour when the time is scaled by τ_p based on the pool properties. The power-law is slightly smaller than 1/2 at $\simeq 0.47$. We therefore predict $r = 1.3 \times R_b(t/\tau_p)^{0.47}$. Similar exponents were observed for coalescence of two drops in Thoroddsen *et al.* (2005*b*) (their figure 22*b*).

The close-up video frames allow us to estimate the apparent interfacial angles at the triple-point, thus allowing us to estimate the instantaneous balance of the three tensions. Figure 6(*b*) shows a close-up of the neck for the lowest drop density (0.65 cSt silicone oil), where the index of refraction is well matched, as seen in

https://doi.org/10.1017/jfm.2014.67 Published online by Cambridge University Press

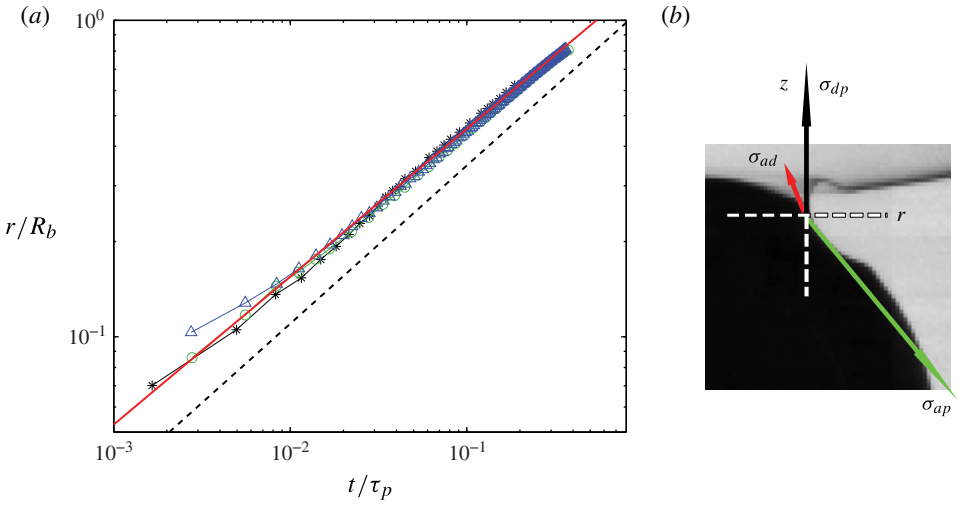


FIGURE 6. (*a*) Radius, versus time, of the contact for bubble transitioning through the interface from salty-water into: 0.65 cSt silicone oil (*); PP1 (blue △); PP90 (green ○). The red line has a slope of 0.47 and the black broken line 0.5. The initial bubble diameters are $\simeq 500$ μm. (*b*) Sketch of the surface tension balance at the triple-line, for the 0.65 cSt silicone oil. The length of the arrows indicates the approximate strength of each tension.

figure 8(*a*). This reveals, as expected, that the tensions are not in equilibrium, with a strong net radial component of 47 dyn cm^{-1}, whereas the vertical component is close to neutral, at only about 2 dyn cm^{-1}.

3.5. *Net surface tension*

One can expect the net surface tension $\Delta\sigma$ to affect the speed of the neck. In figure 7 we compare the two liquid combinations which have the largest difference in $\Delta\sigma$, while the densities and viscosities are kept nearly unchanged. This was accomplished by comparing a drop of 1.7 cSt silicone oil ($\Delta\sigma = 109$ dyn cm^{-1}) to a drop of 2-ethylhexyl-acetate ($\Delta\sigma = 80$ dyn cm^{-1}), both in a salt-solution pool. Figure 7(*a*) compares the radius evolution normalizing the time scale based on drop properties $\tau_d = \sqrt{\rho_d R_b^3/\sigma_d}$. Whereas in figure 7(*b*), by normalizing the time with capillary-inertial time-scale based on pool density and on $\Delta\sigma/2$, i.e. $\tau_{\Delta\sigma} = \sqrt{\rho_p R_b^3(2/\Delta\sigma)}$, the two curves fall on top of each other. There is some slow-down at the onset of the motion but rest of the curves follow a power-law with an exponent of 0.44. For these cases we therefore have

$$\frac{r}{R_b} = 1.23\left(\frac{t}{\tau_{\Delta\sigma}}\right)^{0.44}.$$

3.6. *Effect of drop viscosity*

We have investigated how the drop viscosity affects the coalescing neck speed, by gradually increasing the viscosity of the drop liquid, using silicone oils of viscosities between 0.65 and 1000 cP, while retaining the same salt-water solution in the pool. Figure 8 shows how the shape of the neck changes as the viscosity is varied.

https://doi.org/10.1017/jfm.2014.67 Published online by Cambridge University Press

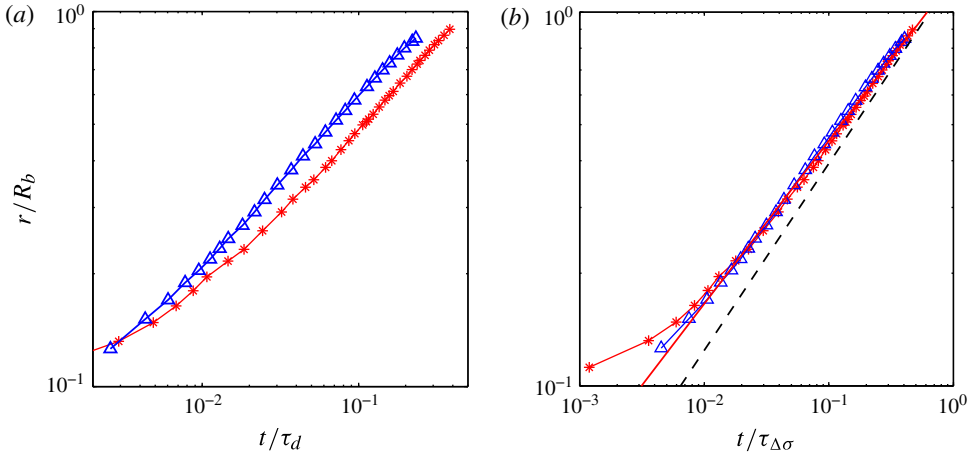


FIGURE 7. Radius versus time for different strength of the net surface tension: for 1.7 cSt silicone oil (△); 2-etylhexyl acetate (*). (*a*) Time normalized by τ_d based on drop properties. (*b*) Time normalized by $\tau_{\Delta\sigma}$ based on the net surface tension. The broken line has a slope of 1/2, whereas the solid line has slope of 0.44.

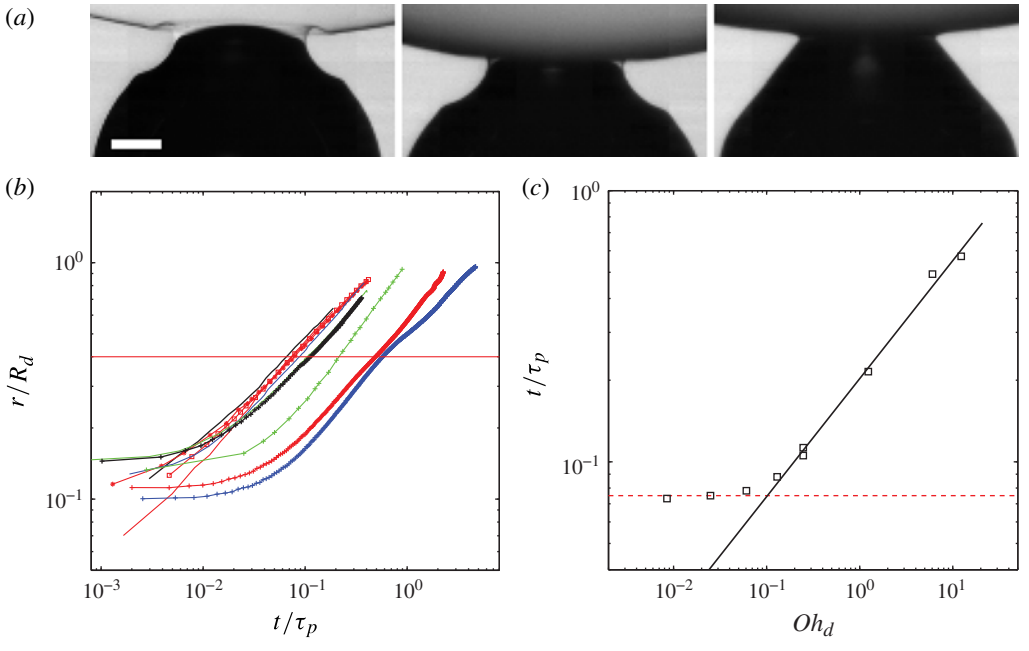


FIGURE 8. The effect of viscosity on the shape and speed of the growing neck. (*a*) Neck shape for three different drop viscosities, $\nu = 0.65$, 5 and 100 cSt (from left to right), shown when $r/R \simeq 0.4$. Scale bar is 100 μm. (*b*) Neck radius versus time for a range of drop viscosities, shown for $\nu =$ 0.65, 1.7, 5, 10, 20, 100, 500, 1000 cSt (from left to right). (*c*) The normalized time when neck radius has grown to 40 % of bubble radius (red line in *a*), versus Ohnesorge number based on drop properties. The time has been normalized by the pool properties in the same way as in figure 5. The horizontal dashed line is at 0.75 and the angled line has a slope of 0.44.

https://doi.org/10.1017/jfm.2014.67 Published online by Cambridge University Press

The neck becomes sharper with increasing viscosity, as was observed for the coalescence of two drops by Thoroddsen *et al.* (2005*b*), Aarts *et al.* (2005) and Paulsen *et al.* (2012). Viscosity has the strongest effects on the earliest neck motions, as shown in figure 8(*b*), with extended initial duration of slow growth, followed by regions where the power-law for all cases is similar, with the same exponent of $\sim 1/2$. This early slow-down is particularly evident for viscosity $\mu_d > 10$ cSt. The initial neck growth rate is greatly slowed down by this effect. To characterize this added friction we look, in figure 8(*c*), at the time required for the neck to reach 40 % of the bubble size. We normalize the viscous effect for the bubble size, in terms of the Ohnesorge number based on the physical properties of the silicone oil $Oh_d = \mu_d/\sqrt{\rho_d \sigma_{ad} R_b}$, where σ_{ad} is here the surface tension between silicone oil and air. For $Oh_d > 0.08$ viscosity significantly slows down the initial motions.

4. Discussion and conclusions

Herein, we have investigated a coalescence configuration involving a triple-line, arising between a bubble and two immiscible liquids, over a wide range of liquid properties. Production of satellites is qualitatively similar to earlier results for bubbles or drops, if we use the net surface tension in the Ohnesorge number. For low-viscosity liquids the growth rate of the coalescing neck is also similar to previous power-laws, with exponents somewhat smaller than 1/2 (Wu *et al.* 2004; Thoroddsen *et al.* 2005*a*,*b*). When the drop viscosity is increased, while the pool remains at low viscosity, we see a strong deviation from this power-law during early times. We suggest that this early slow-down arises from an added friction associated with the triple-line, when the originally co-linear surfaces adjust to the constraint of the contact angles at the triple-line, which forces motion within the viscous liquid inside the drop, leading to added friction. This differs qualitatively from the coalescence dynamics of two miscible drops of different viscosities, where it has been shown that the motion of the lower-viscosity liquid decouples from the high-viscosity one, as in that configuration there is no sharp triple-line (Thoroddsen *et al.* 2007). This highlights a fundamental difference between the coalescence dynamics for immiscible and miscible liquids (Blanchette *et al.* 2009; Thoraval & Thoroddsen 2013). Our configuration can be thought of as the wetting of a bubble. Wetting of a solid surface by a drop has a three-phase contact line, which has recently been shown to provide strong friction (Carlson *et al.* 2012) over a range of viscosities. However, for low viscosities Winkels *et al.* (2012) have shown the earliest spreading to be independent of wettability. More exotic possibilities include free-surface formation as described by Sprittles & Shikhmurzaev (2012). Our configuration may therefore act as a bridge between the various different coalescence scenarios.

Many possible extensions arise from this work. We have mainly restricted our configurations to a low-viscosity pool liquid of salty water, to minimize differences in refractive index. Other configurations include a pool of higher viscosity than the drop, but in this case we do not expect satellite formation. How surfactants affect the dynamics would also be of considerable industrial interest. Surfactants may be soluble in only one of the phases and will affect the three interfacial tensions in different ways producing a wider range of possible $\Delta\sigma$, which may prevent satellite formation. Surfactants can also introduce dynamic surface tension and dampen capillary waves, thereby changing the critical values of Oh. However, such experiments are challenging, as surfactants also tend to prevent the onset of coalescence, a fact of importance in composite emulsions in microfluidics.

https://doi.org/10.1017/jfm.2014.67 Published online by Cambridge University Press

Acknowledgement

EQL is grateful for a SABIC Postdoctoral Fellowship.

Supplementary material

Supplementary materials are available at http://dx.doi.org/10.1017/jfm.2014.67.

References

AARTS, D. G. A. L., LEKKERKERKER, H. N. W., GUO, H., WEGDAM, G. H. & BONN, D. 2005 Hydrodynamics of droplet coalescence. *Phys. Rev. Lett.* **95**, 164503.

BLANCHETTE, F. & BIGIONI, T. P. 2006 Partial coalescence of drops at liquid interfaces. *Nat. Phys.* **2**, 254–257.

BLANCHETTE, F. & BIGIONI, T. P. 2009 Dynamics of drop coalescence at fluid interfaces. *J. Fluid Mech.* **620**, 333–352.

BLANCHETTE, F., MESSIO, L. & BUSH, J. W. M. 2009 The influence of surface tension gradients on drop coalescence. *Phys. Fluids* **21**, 072107.

CARLSON, A., BELLANI, G. & AMBERG, G. 2012 Universality in dynamic wetting dominated by contact-line friction. *Phys. Rev.* E **85**, 045302(R).

CHARLES, G. E. & MASON, S. G. 1960 The mechanism of partial coalescence of liquid drops at liquid/liquid interfaces. *J. Colloid Sci.* **15**, 105–122.

CHEN, X. P., MANDRE, S. & FENG, J. J. 2006 Partial coalescence between a drop and a liquid–liquid interface. *Phys. Fluids* **18**, 051705.

DING, H., LI, E. Q., ZHANG, F. H., SUI, Y., SPELT, P. D. M. & THORODDSEN, S. T. 2012 Propagation of capillary waves and ejection of small droplets in rapid droplet spreading. *J. Fluid Mech.* **697**, 92–114.

DE GENNES, P.-G., BROCHARD-WYART, F. & QUÉRÉ, D. 2004 *Capillarity and Wetting Phenomena: Drops, Bubbles, Pearls, Waves*. Springer.

GILET, T., MULLENERS, K., LECOMTE, J. P., VANDEWALLE, N. & DORBOLO, S. 2007 Critical parameters for the partial coalescence of a droplet. *Phys. Rev.* E **75**, 036303.

HONEY, E. M. & KAVEHPOUR, H. P. 2006 Astonishing life of a coalescing drop on a free surface. *Phys. Rev.* E **73**.

MOHAMED-KASSIM, Z. & LONGMIRE, E. K. 2004 Drop coalescence through a liquid/liquid interface. *Phys. Fluids* **16**, 2170–2181.

NEESON, M. J., TABOR, R. F., GRIESER, F., DAGASTINE, R. R. & CHAN, D. Y. C. 2012 Compound sessile drops. *Soft Matt.* **8**, 11042–11050.

OHNISHI, M., AZUMA, H. & STRAUB, J. 1999 Study on secondary bubble creation induced by bubble coalescence. *Adv. Space Res.* **24**, 1331–1336.

PAULSEN, J. D., BURTON, J. C. & NAGEL, S. R. 2011 Viscous to inertial crossover in liquid drop coalescence. *Phys. Rev. Lett.* **106**, 114501.

PAULSEN, J. D., BURTON, J. C., NAGEL, S. R., APPATHURI, A., HARRIS, M. T. & BASARAN, O. A. 2012 The initial regime of coalescence: the inexorable resistance of inertia. *Proc. Natl Acad. Sci. USA* **109**, 6857–6861.

RAY, B., BISWAS, G. & SHARMA, A. 2010 Generation of secondary droplets in coalescence of a drop at a liquid–liquid interface. *J. Fluid Mech.* **655**, 72–104.

RIOBOO, R., ADAO, M. H., VOUE, M. & DE CONINCK, J. 2006 Experimental evidence of liquid drop break-up in complete wetting experiments. *J. Mater. Sci.* **41**, 5068–5080.

ROUX, D. C. D. & COOPER-WHITE, J. J. 2004 Dynamics of water spreading on a glass surface. *J. Colloid Interface Sci.* **277**, 424–436.

SMEDLEY, G. & COLES, D. 1990 Some transparent immiscible liquid pairs. *J. Colloid Interface Sci.* **138**, 42–60.

SPRITTLES, J. E. & SHIKHMURZAEV, Y. D. 2012 Coalescence of liquid drops: different models versus experiment. *Phys. Fluids* **24**, 122105.

https://doi.org/10.1017/jfm.2014.67 Published online by Cambridge University Press

THORAVAL, M.-J. & THORODDSEN, S. T. 2013 Contraction of an air disk caught between two different liquids. *Phys. Rev.* E **88**, 061001(R).

THORODDSEN, S. T., ETOH, T. G., TAKEHARA, K. & OOTSUKA, N. 2005*a* On the coalescence speed of bubbles. *Phys. Fluids* **17**, 071703.

THORODDSEN, S. T., QIAN, B., ETOH, T. G. & TAKEHARA, K. 2007 The initial coalescence of miscible drops. *Phys. Fluids* **19**, 072110.

THORODDSEN, S. T. & TAKEHARA, K. 2000 The coalescence-cascade of a drop. *Phys. Fluids* **12**, 1257–1265.

THORODDSEN, S. T., TAKEHARA, K. & ETOH, T. G. 2005*b* The coalescence speed of a pendent and a sessile drop. *J. Fluid Mech.* **527**, 85–114.

WINKELS, K. G., WEIJS, J. H., EDDI, A. & SNOEIJER, J. H. 2012 Initial spreading of low-viscosity drops on partially wetting surfaces. *Phys. Rev.* E **85**, 055301(R).

WU, M., CUBAUD, T. & HO, C.-M. 2004 Scaling law in liquid drop coalescence driven by surface tension. *Phys. Fluids* **16**, L51.

YUE, P. T., ZHOU, C. F. & FENG, J. J. 2006 A computational study of the coalescence between a drop and an interface in Newtonian and viscoelastic fluids. *Phys. Fluids* **18**, 102102.

ZHANG, F. H., LI, E. Q. & THORODDSEN, S. T. 2009 Satellite formation during coalescence of unequal size drops. *Phys. Rev. Lett.* **102**, 104502.

ZHANG, F. H. & THORODDSEN, S. T. 2008 Satellite generation during bubble coalescence. *Phys. Fluids* **20**, 022104.

https://doi.org/10.1017/jfm.2014.67 Published online by Cambridge University Press